

## Supplementary Information for

# Ni Crossover Catalysis: Truth of Hydrogen Evolution in Ni-rich Cathode-based Lithium-ion Batteries

Xingqin Wang <sup>1,3</sup>, Dongsheng Ren <sup>2</sup>, Hongmei Liang <sup>2</sup>, Youzhi Song <sup>2</sup>, Hua Huo <sup>1,\*</sup>, Aiping Wang <sup>2,\*</sup>, Yunzhi Gao <sup>1</sup>, Jianhong Liu <sup>2</sup>, Yun Gao <sup>2</sup>, Li Wang <sup>2,\*</sup>, Xiangming He <sup>2,\*</sup>

<sup>1</sup> Key Laboratory of Materials for New Energy Conversion and Storage (Ministry of Industry and Information Technology, School of Chemistry and Chemical Engineering, Harbin Institute of Technology, Harbin, 150001, China.

<sup>2</sup> Institute of Nuclear and New Energy Technology, Tsinghua University, Beijing, 100084, China

<sup>3</sup> Risesun Mengguli New Energy Science and Technology Co., LTD, Beijing, 102200, China

\* Corresponding author.

E-mail addresses: huohua@hit.edu.cn; aipingwang\_aw@outlook.com; wang-l@tsinghua.edu.cn; hexm@tsinghua.edu.cn.

## Supplementary Figures and Tables

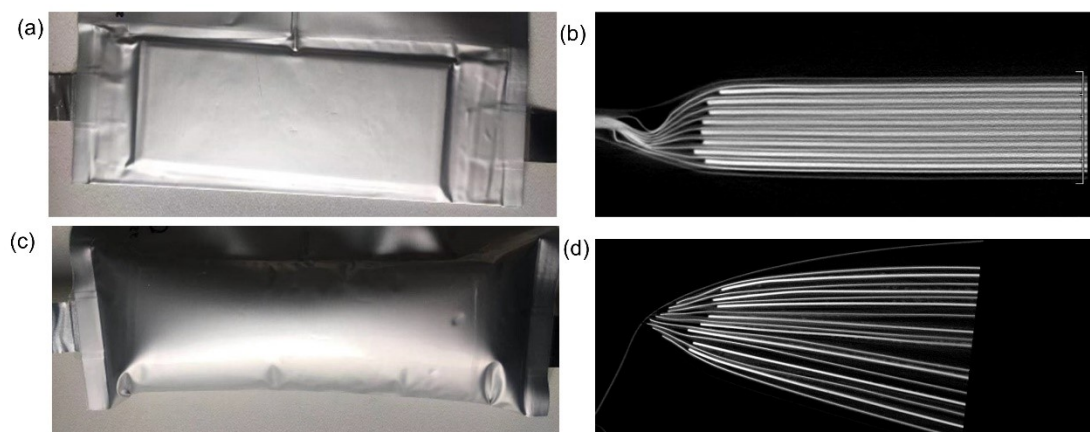


Figure S1. (a) Optical appearance and (b) industrial computerized tomography (CT) image of the cross-section of the fresh NMC622//Gr cell. (c) Optical appearance and (d) CT image of the cross-section of the cell after 790<sup>th</sup> cycles. As can be seen, electrode layers in the fresh cell aligned well with each other. In contrast, the electrode layers in the dead cell were expanded by the accumulated gas.

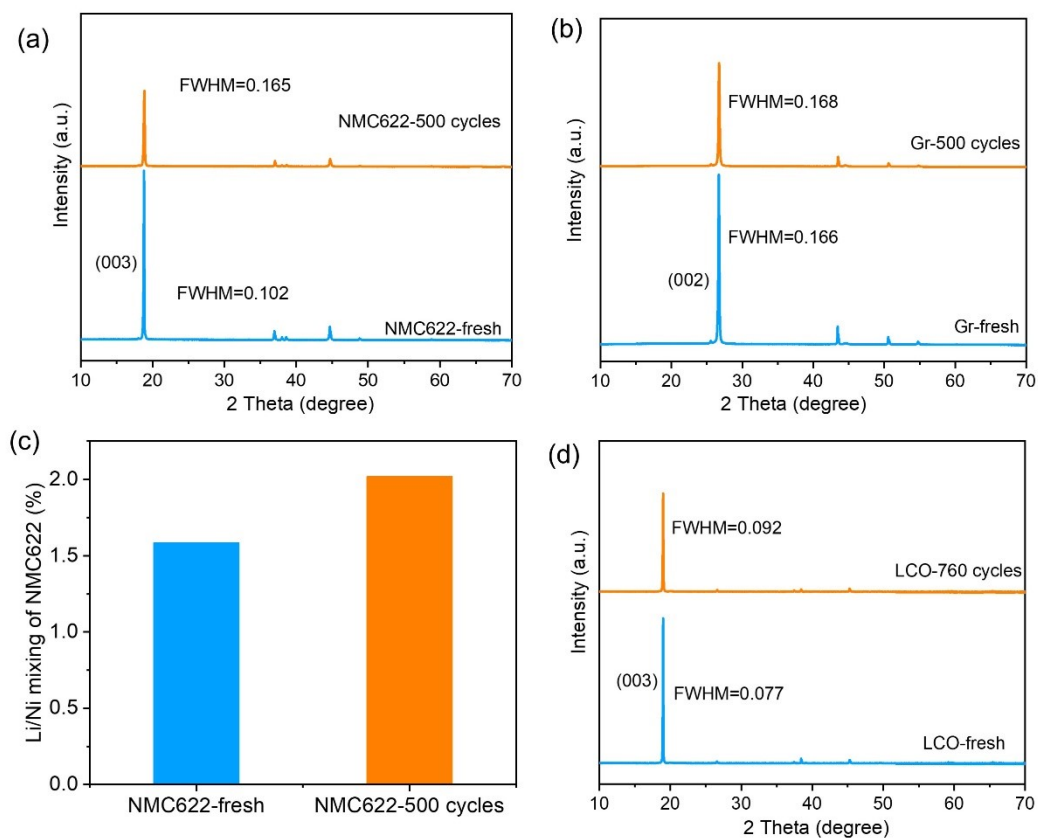


Figure S2. Rietveld refined X-ray diffraction (XRD) of electrodes before and after cycling. XRD of (a) NMC622 and (b) Gr in NMC622//Gr battery. (c) Li/Ni mixing in NMC622 cathodes. (d) XRD of LCO cathode. Full width half maximums (FWHMs) of peaks of are noted.

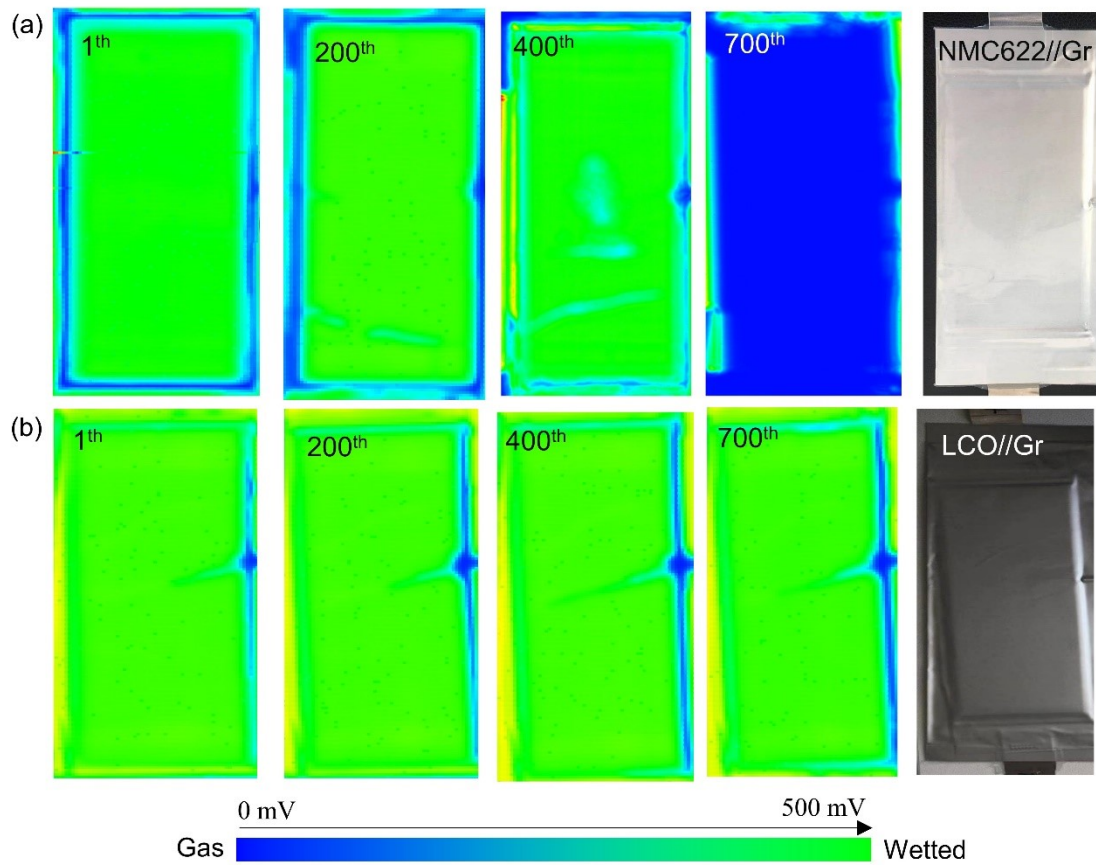


Figure S3. Ultrasonic scanning images of (a) NMC622//Gr and (b) LCO//Gr cells at different cycles. The blue indicates gas evolution. The cells of 5 Ah were used here.

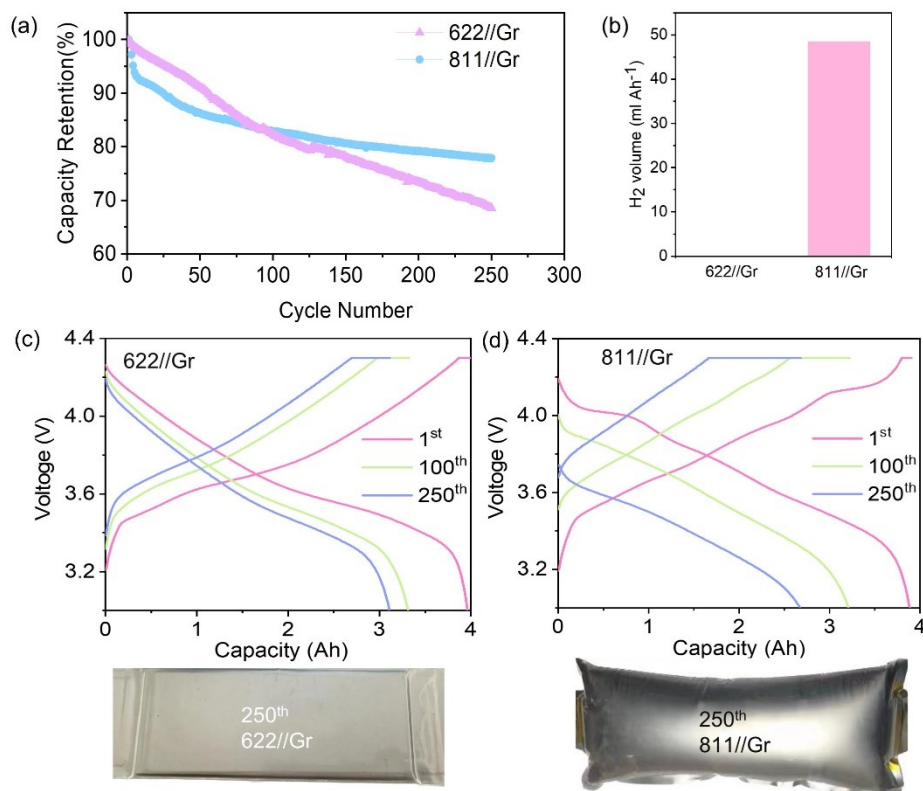


Figure S4. Cycling performance and gas evolution of pouch cells with cathodes having different content of Ni. (a) Cycling performance of NMC622//Gr (622//Gr) and NMC811//Gr (811//Gr) cells. (b) H<sub>2</sub> evolution per 1 Ah capacity of each cell, which was measured by gas chromatography (GC). (c-d) Voltage-capacity cycles and the optical images after long-term cycling of the cells. The cells were cycled at 1C between 3.0 – 4.3 V at 55 °C. The high temperature was used to expedite the aging of batteries.

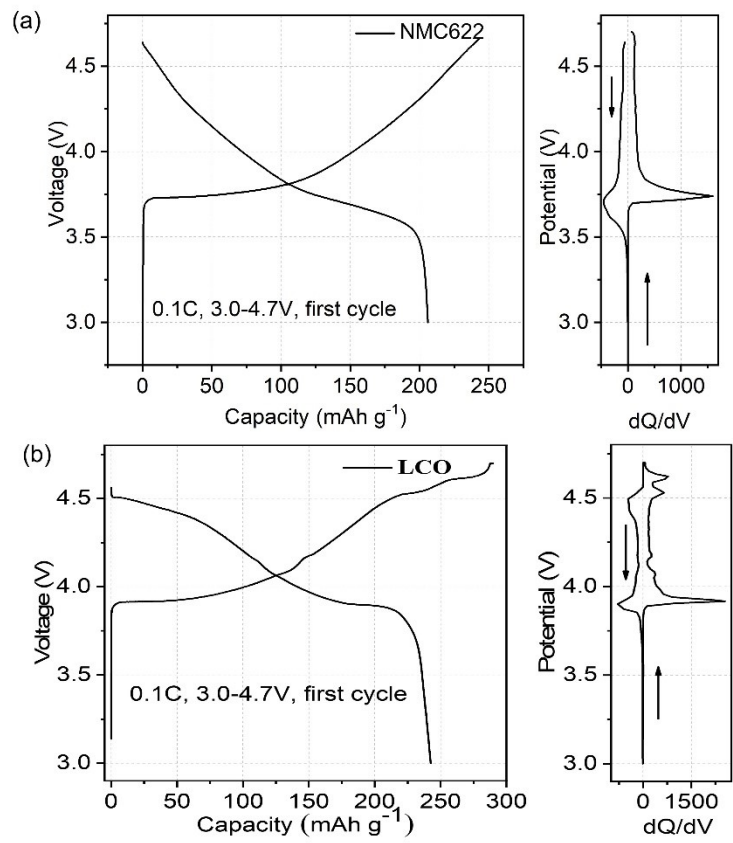


Figure S5. Voltage-Capacity and the dQ/dV curves of (a) NMC622//Li and (b) LCO//Li half cells at 0.1 C in the voltage range of 3.0 – 4.7 V vs. Li<sup>+</sup>/Li.

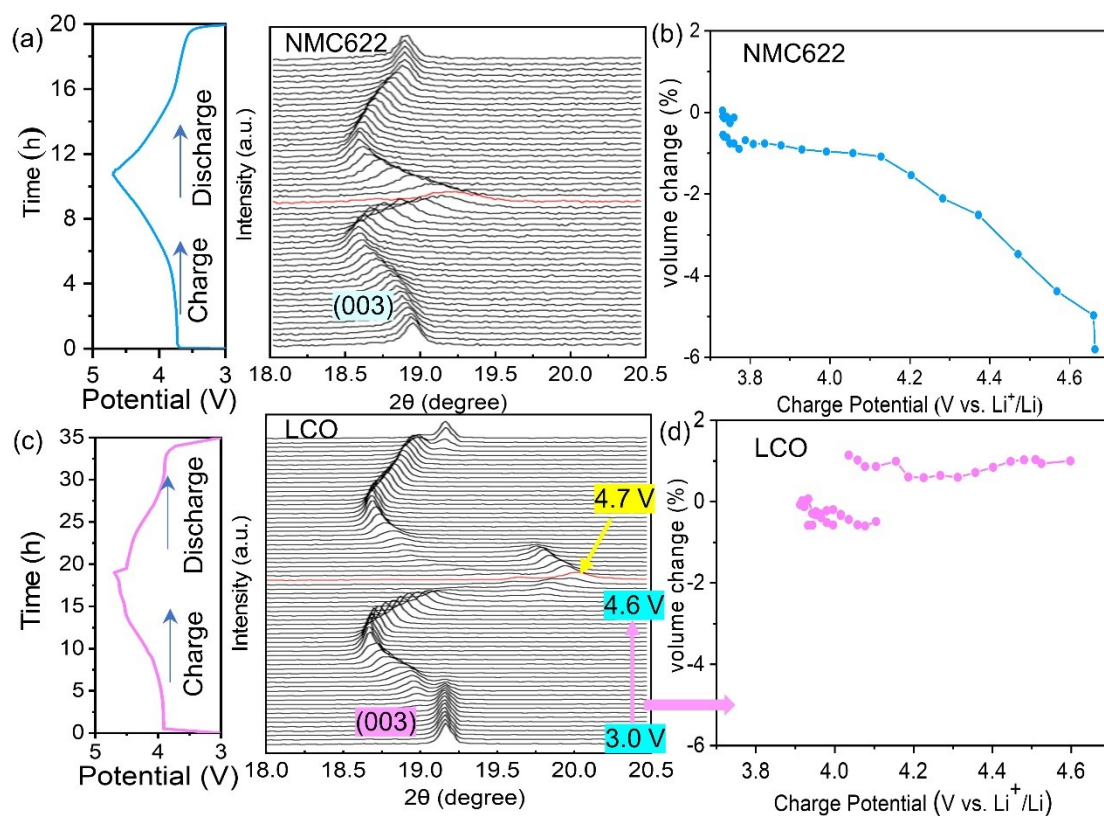


Figure S6. Crystal structure evolution and volume change during the first cycle of NMC622//Li and LCO//Li half cells in the voltage range of 3.0 - 4.7 V. Evolution of (003) diffraction peaks of NMC622 (a) and LCO (c) characterized by operando XRD, as well as the crystal volume changes of NMC622 (b) and LCO (d) as a function of the voltage. Note only the volume variation of LCO under 4.6 V is considered.

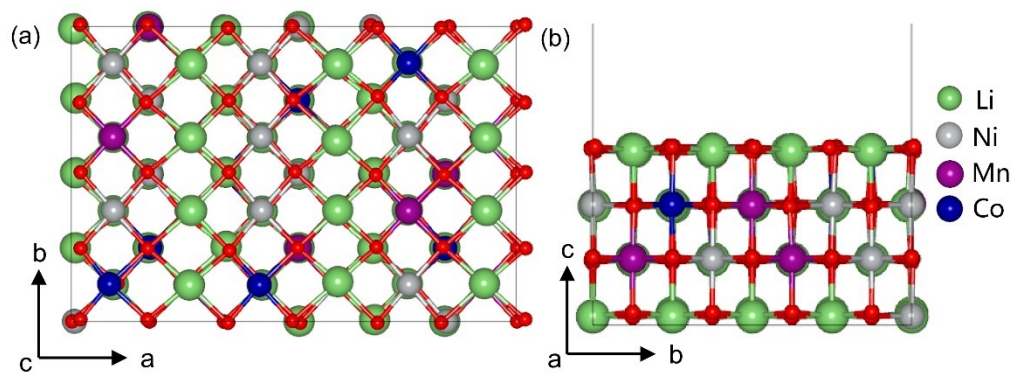


Figure S7. The four layer surface model of  $\text{Li}_{48}(\text{Ni}_{28}\text{Mn}_{10}\text{Co}_{10})\text{O}_{96}$ . (a) top view, (b) side view. The  $c$  direction is  $[10\bar{1}4]$ .



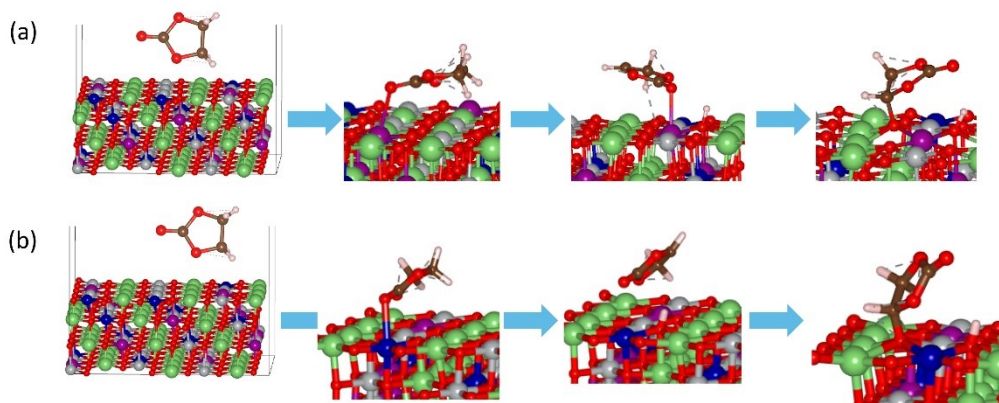


Figure S8. H-transfer process of EC at the (a) Mn and (b) Co sites on NMC622 ( $10\bar{1}4$ ) surface. The color code is as follows: Li-green, Ni-grey, Mn-purple, Co-blue, O-red, C-brown, H-pink.

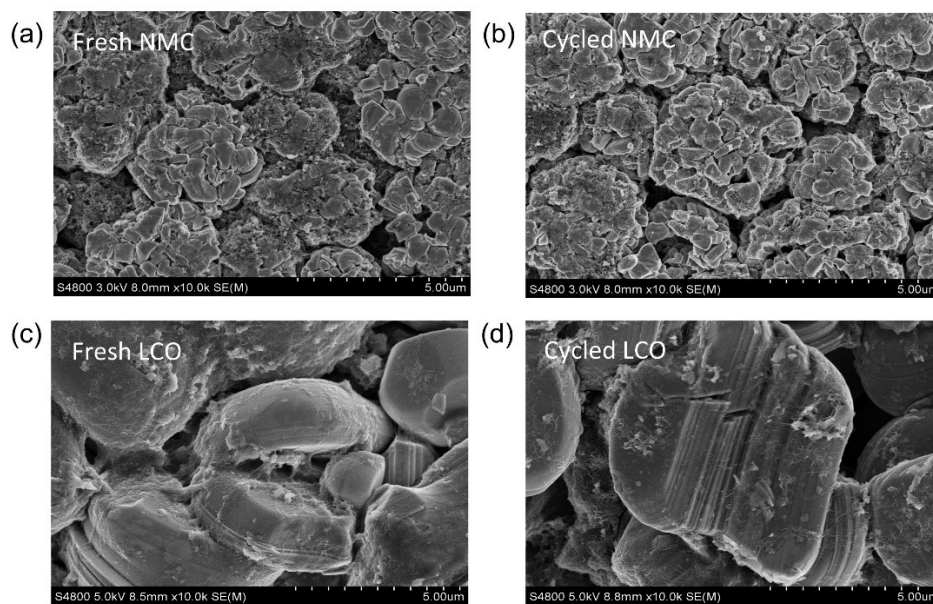


Figure S9. SEM images of the fresh (a, c) and cycled (b, d) NMC622 and LCO cathodes. Note that the disassembled cells were at the end of life (EOL). The NMC622 exhibited a much higher specific area than LCO and more active sites were exposed to the electrolyte. Thus, significant side reactions would occur at the NMC622 cathode/electrolyte interface.

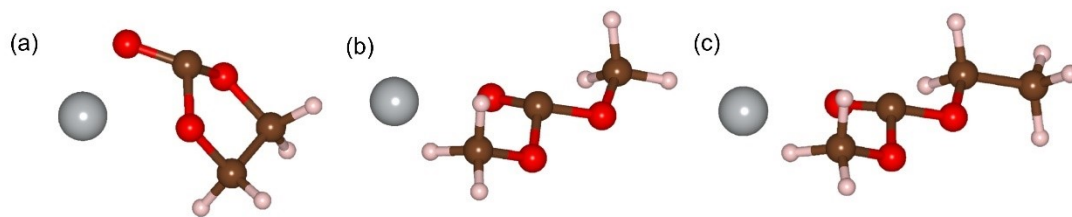


Figure S10. Reduced solvent geometries with Ni around in a ball-and-stick model. Color code: Ni-grey, O-red, C-brown, H-pink.

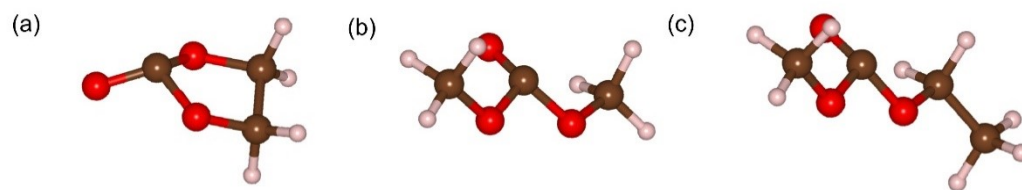


Figure S11. Reduced solvent geometries without Ni around in a ball-and-stick model. Color code: O-red, C-brown, H-pink.

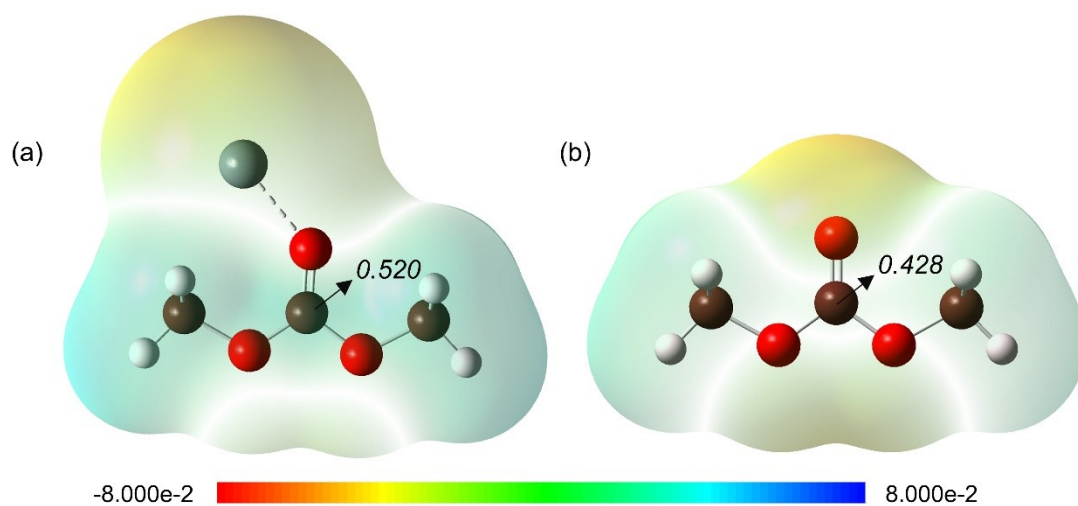


Figure S12. Electrostatic potential of DMC with (a) and without (b) Ni around. The Mulliken charge of the carbonyl carbon is marked on the contour surface structure. Color code: O-red, C-brown, H-pink.

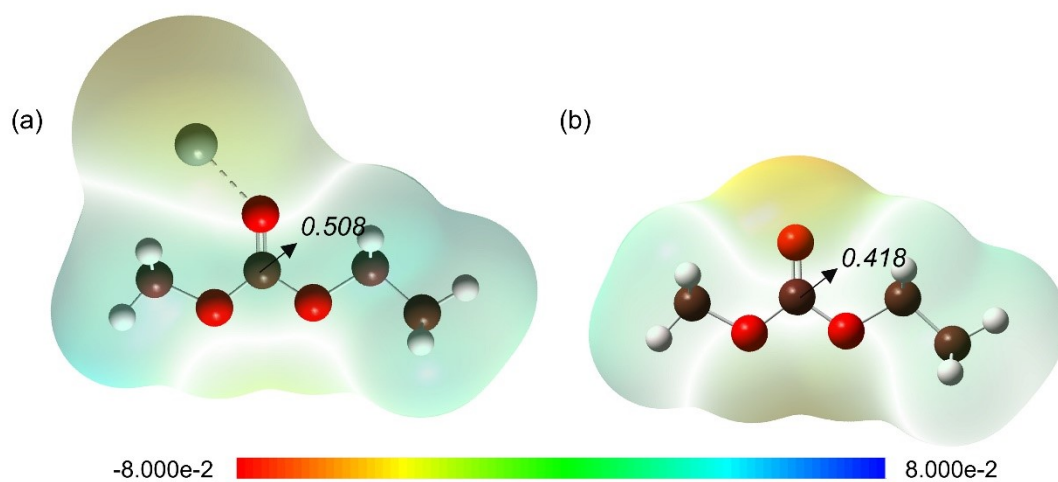


Figure S13. Electrostatic potential of EMC with (a) and without (b) Ni around. The Mulliken charge of the carbonyl carbon is marked on the contour surface structure. Color code: O-red, C-brown, H-pink.

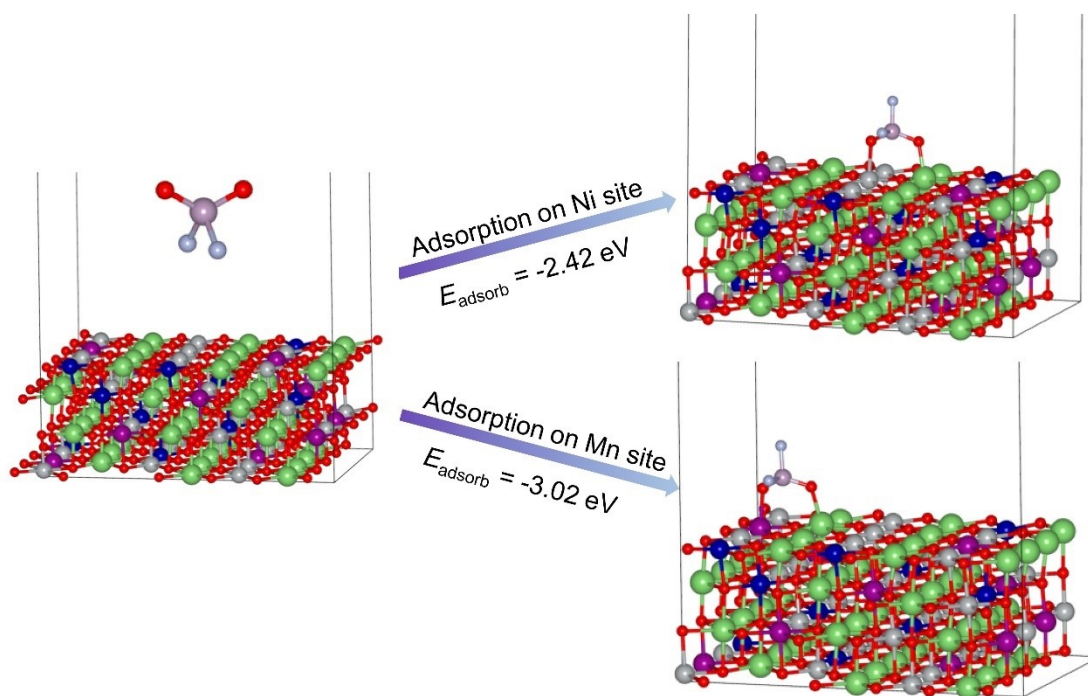


Figure S14. Adsorption energy of the additive ( $\text{PO}_2\text{O}_2$ ) on the active site on NMC622 surface, where both the Ni and Mn sites are considered. The adsorption energy is calculated by  $E_{\text{adsorb}} = E_{\text{PO}_2\text{F}_2@622} - E_{622} - E_{\text{PO}_2\text{F}_2}$ . The strong adsorption of the additive on the active site on NMC622 surface prevents the solvent (like EC) adsorption, avoiding the catalysis of the surface active site toward the H-transfer, which not only protect the electrolyte, but also stabilize the NMC cathode and prohibit the TM dissolution and gassing.

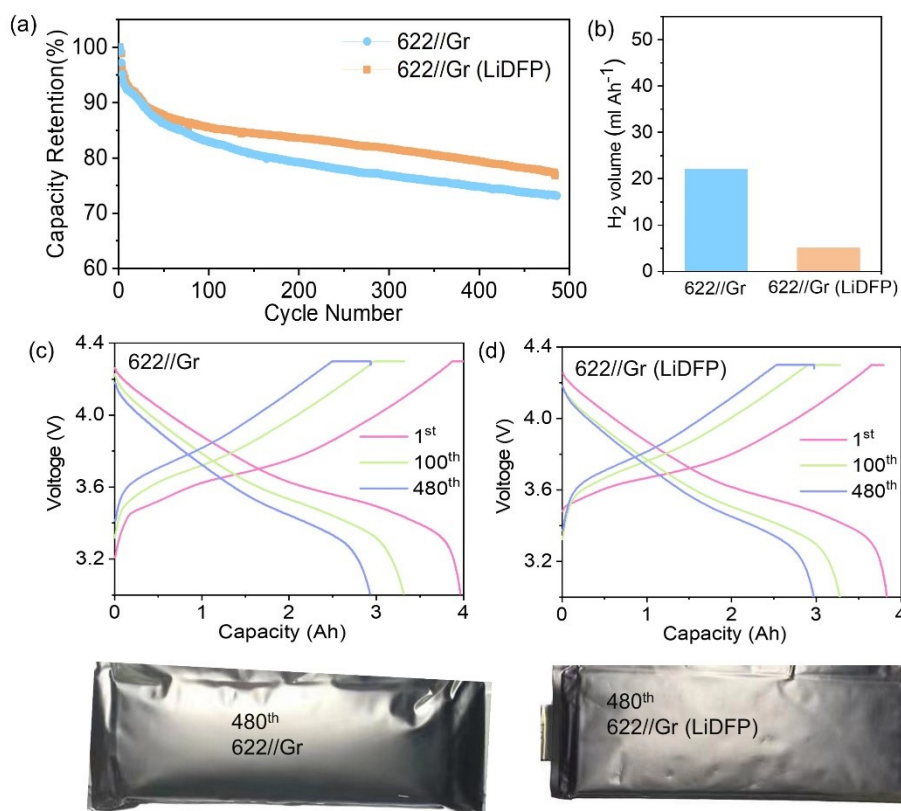


Figure S15. Cycling performance and gas evolution of the NMC622//Gr pouch cells with and without LiDFP. (a) Cycling performance. (b) H<sub>2</sub> evolution per 1 Ah capacity of each cell, which was measured by gas chromatography (GC). (c-d) Voltage-capacity cycles and the optical images after long-term cycling of the cells. The cells were cycled at 1C between 3.0 – 4.3 V at 55 °C. The high temperature was used to expedite the aging of batteries.



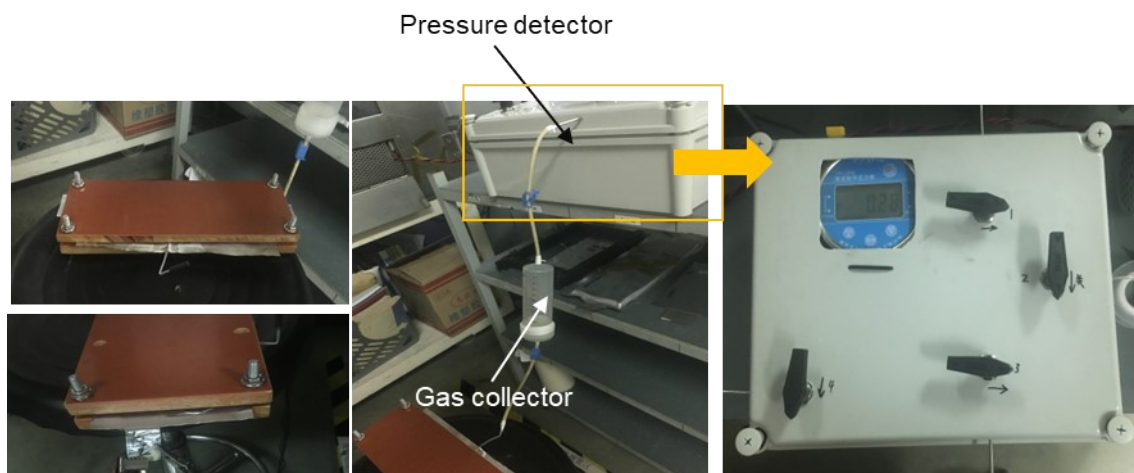


Figure S16. Home-made operando gas volume detector based on the ideal gas law  $pV=nRT$ , in which  $p$  is the pressure,  $V$  the volume,  $n$  the number of moles,  $R$  the gas constant, and  $T$  the temperature. Once the gas was evolved in the pouch cell, it flowed to the gas collector due to the pressure of the plates.

Table 1. Detailed information of ~ 50 Ah NMC622//Gr and LCO//Gr pouch cells with a capacity of used in this study.

| Cell chemistry                            | NMC622//Gr  |         | LCO//Gr |         |
|---|---|---------|---------|---------|
|   | NMC622  | Gr      | LCO     | Gr      |
| Active material                           | Al foil   | Cu foil | Al foil | Cu foil |
| Current collector                         | Al foil   | Cu foil | Al foil | Cu foil |
| Capacity (mAh g <sup>-1</sup> )           | 175   | 360     | 160     | 360     |
| Coating weight (g m <sup>-2</sup> )       | 400   | 220     | 425     | 220     |
| Calendering density (g cc <sup>-1</sup> ) | 3.5   | 1.58    | 3.5     | 1.58    |
| Electrolyte                               | 1 M LiPF <sub>6</sub> in the mixture of EC/EMC/DMC (1 : 1 : 1 by volume) with 1 wt% VC. |         |         |         |
| Cell size                                 | Length (227 mm) × Width (161 mm) × Height (~12 mm)                                      |         |         |         |

Table 2. Detailed information of ~ 5 Ah NMC622//Gr and NMC811//Gr pouch cells used in this study.

| Cell chemistry                            | NMC622//Gr  |         | 811//Gr |         |
|---|---|---------|---------|---------|
|   | NMC622  | Gr      | 811     | Gr      |
| Active material                           | Al foil   | Cu foil | Al foil | Cu foil |
| Current collector                         | Al foil   | Cu foil | Al foil | Cu foil |
| Capacity (mAh g <sup>-1</sup> )           | 175   | 360     | 205     | 360     |
| Coating weight (g m <sup>-2</sup> )       | 400   | 220     | 345     | 220     |
| Calendering density (g cc <sup>-1</sup> ) | 3.5   | 1.58    | 3.4     | 1.55    |
| Electrolyte                               | 1 M LiPF <sub>6</sub> in the mixture of EC/EMC/DMC (1 : 1 : 1 by volume) with 1 wt% VC. |         |         |         |
| Cell size                                 | Length (190 mm) × Width (65mm) × Height (~4 mm)   |         |         |         |